Online Wireless Lab Testbed

Martin Danneberg*, Roberto Bomfin*, Shahab Ehsanfar*, Ahmad Nimr*, Zhitao Lin*,
Marwa Chafii†, Gerhard Fettweis*
*Vodafone Chair Mobile Communication Systems, Technische Universität Dresden, Germany
†ETIS UMR 8051, Université Paris Seine, Université de Cergy-Pontoise, ENSEA, CNRS, France
*{first name.last name}@ifn.et.tu-dresden.de, marwa.chafii@ensea.fr

***Abstract*—This paper describes the remote accessible Online Wireless Lab (OWL) Testbed. The aim is to set-up a flexible yet real-time test infrastructure based on the *National Instruments* USRP-RIO software-defined radio platform. The testbed is located indoor and outdoor on the campus of TU Dresden, Germany. Access and reconfiguration of relevant parts of the cellular network are granted and allow to conduct physical and higher network layer experiments.**

***Index Terms*—Testbed, SDR, Outdoor, Indoor, Measurements, Evaluation, Infrastructure, Experimentation.**

I. Introduction

The requirements of future wireless applications differ greatly between higher data rates for enhanced Mobile BroadBand (eMBB), ultra-reliable low latency communication (URLLC), and massive machine-type communications. To satisfy these demands, several attempts [1] have been made to propose suitable waveforms and many studies focus on improving the network layers and applications. However, achieving the complex requirements is only possible when all network layers are jointly optimized rather than individually [2].

In general, most research consider assumptions to simplify the models and rely on simulation to evaluate the performance. For instance, in many cases the radio-frequency (RF)-front end is considered linear. However, highly-linear and power-inefficient power-amplifiers are affordable for the base-station (BS), not necessarily for the user-terminal (UT). Another example is when the whole physical layer (PHY) is abstracted to study the higher network layers. Usually oversimplifications tend to be unrealistic. One of the common assumptions is perfect synchronization, which has a very critical influence on the performance and is a challenging task in practice. Further, simulations are normally carried out in floating point, whereas fixed-point is applied in hardware.

In the past decade, many testbeds were built, capturing different aspects of communication networks. The testbeds can be roughly grouped:

- "PHY" testbeds concentrate on the PHY layer and often perform link-level experiments, evading the challenges concerning multiple users and higher network protocols.
- "MAC" testbeds with the interest in performing experiments on local wireless networks with many clients. Thus, standard-compliant MAC-PHY platforms (e.g. WiFi or Zigbee-Cards) are used to abstract the challenges at the lower network layers [3]. Or USRP-similar platforms are utilized to offload the PHY to host-based signal processing [4], keeping the flexibility by increasing the latency and reducing the throughput.
- "Network" testbeds [5], which emulate a massive amount of nodes without wireless connections to target evaluating network performance in general.

Due to the scarcity of the radio spectrum, many wireless testbeds are located indoor, using shielded environments, or the outdoor section is available on request and requires the physical presence of the experimenter [6]. Thus, the aim of our presented testbed is to mix these three categories to enable research on cellular networks ranging from the PHY layer to the application layer. The following sections give a detailed description of the testbed. First, in Section II, the layout of the testbed is presented. In subsection II-A and II-B, we detail the hardware set-up, followed by the software environment for remote control. A first trial evaluation of the testbed is given in Section III. Finally, we conclude the paper in Section IV.

II. Architecture

The cellular testbed [7] has two types of nodes mounted permanently: 1) Six indoor nodes mounted on the ceiling. 2) four outdoor sites referred as BS mounted on the rooftop of the university buildings. Both node types are equally equipped to use them as either BS or UT. The indoor nodes can hold one set of software-defined radio (SDR) devices, whereas the BS can hold multiple. The geographical layout of the testbed at Barkhausen-Bau of TU Dresden is shown in Fig. 1. Beside the mounted nodes, two laboratory rooms (LR) are connected to the testbed to flexibly add nodes. Further, several bicycle rickshaws and one robot platform are available as mobile nodes for intended experimentation.

The testbed has a transmission license from the German regulator Bundesnetzagentur with 100 MHz Bandwidth at 3.75 GHz. This band is available in Germany for campus networks and is close to the 5G frequencies. The license covers outdoor time division multiple access (TDMA) transmissions of up to 10 Watt equivalent isotropically radiated power (EIRP) in a 10 km radius around the university campus.

This work is supported by *National Instruments (NI)* and *Hewlett Packard Enterprise (HPE)* with hardware, software and technical support. This project has received funding from the European Union's Horizon 2020 research and innovation programme under grant agreement No 732174 (ORCA).

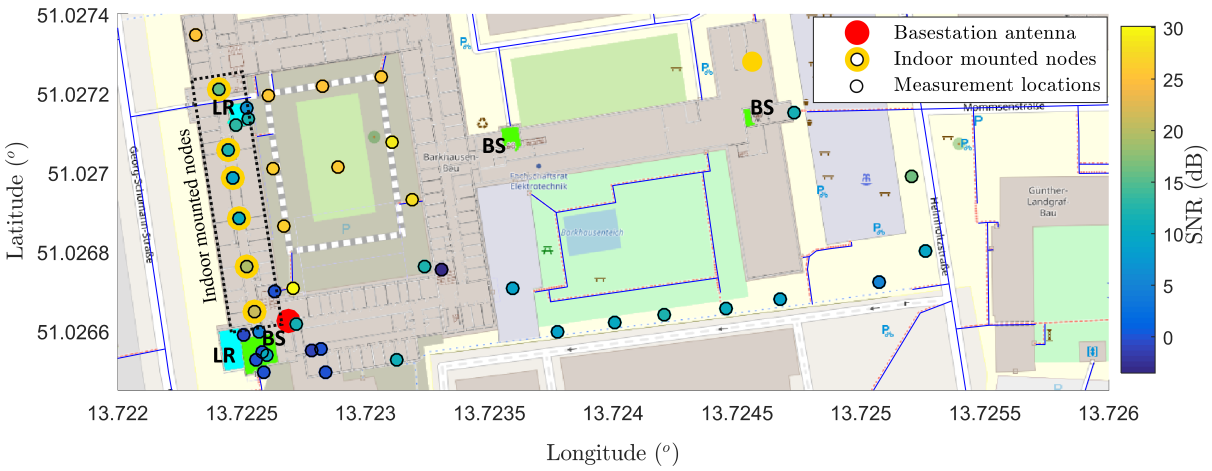

Fig. 1: Layout of the testbed using Open Street Map Data [8]. Nodes on roof-top level are filled in green. A fourth base-station is located on another building and is not included in the map. The two laboratory rooms are filled in light blue.

A. Hardware

The hardware in the testbed is selected to be as generic as possible, but providing sufficient processing power. The USRP-RIO series from *National Instruments (NI)* accomplish that by connecting a *Xilinx* KINTEX 7 FPGA to two independent, broadband radios. A *NI* USRP-RIO can be converted into a *Ettus* USRP X310, such that many open and closed software frameworks are compatible [9]. As shown in Fig. 2, each node consists of one USRP-2974 and one USRP-RIO to provide two independent SDR platforms. Further, the USRP-2974 encompasses an Intel i7 host platform, where each USRP is connected via PCIe. To enhance the SDR platform with sensing capabilities one additional USRP B205-mini is attached to the USRP 2974 via USB3. All the selected USRPs provide a frequency range from 10 MHz to 6 GHz. Therefore, the aim is to provide each SDR a broadband RF front-end, which is powerful enough for micro cell experiments. The covered bands should include both WiFi-bands and the 3.75 GHz band. As a result, the selected RF components need to cover the frequency range from 2 up-to 6 GHz.

Since the power output of the USRP degrades with higher frequency and to compensate the cable and filter losses, the 1 Watt ZVE-8G+ power amplifier from *Mini-Circuits* is chosen, for being broadband and highly linear. However, one drawback of using a transmitter (TX) power amplifier is the sensitivity of the receiver. The allowable USRP input power is -15 dBm. Thus, the isolation between transmit and receive chain must be at least 45 dB. To achieve this, several options are available:

- Typical frequency multiplexing system cover this using band-pass filters and a frequency gap between uplink (UL) and downlink (DL).
- In radar applications also RF circulators are used.
- Using a switch to select the operation mode is common in in TDMA systems.

Several band-passes and switches were tested during the planning phase of the testbed. The common requirements are: 1) capability to handle 1 Watt of input power, 2) a low insertion loss of less than 3 dB, 3) enough isolation between the transmit and receive part and 4) being broadband for flexible usage. To provide very generic and reproducible results, Commercial off-the-shelf (COTS) equipment is to be used rather than customized front-ends. Considering low-cost also for the selection of the components, the following options are viable:

- *G-Way Microwave* offers a custom filter design meeting the requirements with more than 50 dB isolation, however the front-end will be bandwidth limited and the UL and DL frequencies has to be fixed.
- Circulators are typically expensive and only military-grade components meet the requirements, most available products deliver an isolation between 14 and 25 dB.
- RF switches are available in large quantities, much less can offer the specific requirements while keeping a sufficient switching speed.

Two candidate switches are ZSW2-63DR+ and ZFSWA2R-63DR+ from *Mini-Circuits*. The first one is a reflective switch, that appears as an open load to the amplifier and would therefore inflicts damage. Whereas, the other can barely handle 1 Watt power, but provides much better isolation. Hence, three ZSW2-63DR+ switches are combined to meet the requirements as shown in Fig. 2. The first switch terminates the amplifier to a $50\,\Omega$ termination block, to ensure that the output is not open. In case a transmit signal has to be radiated then the first switch routes the signal to a second switch, where the antenna is connected either to the TX or receiver (RX) front-end. Finally, the last switch passes the received signal to the RX or terminates the signal path in case the TX is operating. The goal of the two last switches is to increase the isolation between the two signal paths.

Another method to provide isolation between TX and RX is to place the respective antennas with distance from each other. Omni-directional antennas, like the *MobileMark* MGRM-WHF, have their ”blind” spots along the axis. Placing them close with $180\,^\circ$ angle to each other have an isolation of around

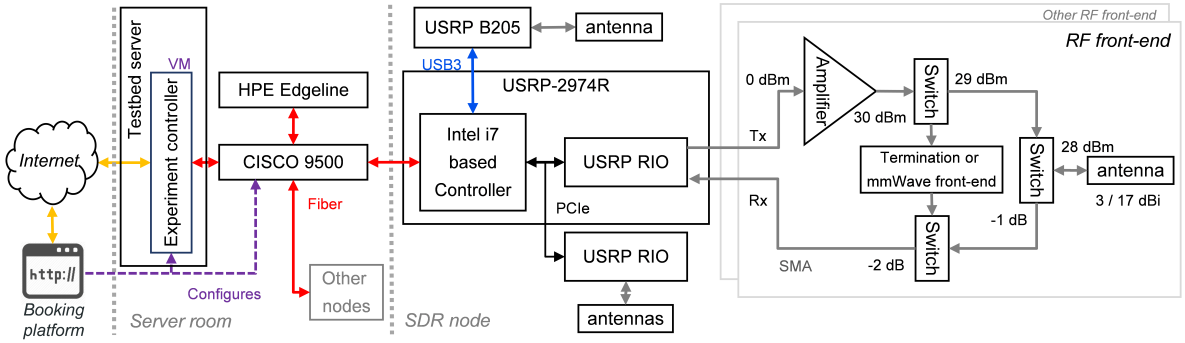

Fig. 2: Testbed component overview

30 dB, depending on the environment. A combination one TX and RX switch would cover the isolation requirements as well. Still, the isolation needs to be verified on the installation spot.

In principle, the set-up between BSs, the indoor and the mobile nodes does not differ. Except that the BSs have sectorized antennas (*Ubiquiti* AM-3G18-120), an additional bandpass filter from *G-Way Microwave* for the transmit signal and GPS synchronized reference clocks. All the SDR nodes are connected to a central server room via fiber cables and a *CISCO* 9500-48Y4C switch. Each indoor node in the testbed has 4 and each outdoor BS 8 fibers. To enable edge cloud computing, several *HPE* edgeline chassis and m710 blades are housed in the central server room. These blades can be booked as part of the experiment.

In addition, a 26 GHz mmWave front-end for the USRP [10] can be added. In contrast to other mmWave-Demonstrators, 2.4 GHz is used as an intermediate frequency, such that the signal processing can be done in the USRP-2944R/X310. The front-end itself converts the signals to 26 GHz. The beam-steering is handled by a 16x16 Butler-Matrix and the built-in antennas. At the receiver side, the signals are down-converted to 2.4 GHz for the USRP receiver. In this way, any USRP X310 compatible software component can be used in the mmWave bands. Since beam-steering is one of the key components compensating the transmission losses by radiating the signal in the preferred direction, the Butler-Matrix has 16 inputs and outputs corresponding to individual 16 beams. This leaves two ways to attach the USRP. One is a 1 to 16 switch, like the *Mini-Circuits* USB-1SP16T-83H, to ”mechanically” steer the beam. The other solution is to connect several USRPs like the *NI* Massive MIMO demonstrator. The first method is simpler and provides basic mmWave functionality, while the other allows spatial multiplexing at the cost of much higher complexity. In the latter, *NI* provides a Massive MIMO software framework.

B. Software

The aim of the testbed is to enable individual experimentation. The working principle of the testbed remote control is outlined in Fig. 2. First, a registered user has to book the nodes needed for the experiment. Afterwards, access to the testbed control server is granted. Here, each user or user group get their own virtual machine (VM) with the experiment control server to store all data and hardware images. The testbed control logic configures the central switch to provide an individual VLAN for the virtual server and the booked resources. Since the testbed is integrated into the Fed4Fire federation, jFed is used to configure the experiment in details. The user can specify which hard-disk image to be copied on the computer of each node and can, therefore, select the operating system and software frameworks for the experiment. Currently Ubuntu & GNU-Radio, Windows & LabVIEW and the NI real-time Linux are supported and tested. The login to the VM is achieved by remote desktop. The control from the VM to the nodes is up to the user. After the experiment, all hard-disk images are copied back to the VM.

Several software frameworks have been tested. From NI, the LTE Application Framework [11] and the 802.11 Application Framework [12] are supported. The open source implementation of the flexible generalized frequency division multiplexing (GFDM) transceiver [13] as well as the WilDCAT Project [14] are available for studying the characteristics of diverse waveforms. Since the experiment control server is virtual, control frameworks like OMF can also be used.

C. Use-cases

The layout with fixed indoor and outdoor UT and BS allows remote controlled experiments without a need of physical presence of the experimenter or mobile devices. The described testbed can be used to study different wireless network scenarios. The key components are: two independent USRPs, one additional USRP for sensing, a powerful host machine and a dedicated fiber network with attached cloud computing platforms. The nodes are generic, such that a compatible USRP(-RIO) firmware can be loaded. Therefore, the testbed is suitable for experiments concerning Multiple Radio Access Technology (Multi-RAT), where the data is split between different PHY/MAC techniques to ensure either a robust communication or to enhance the data rate. Moreover, multi-connectivity experiments are well suited for the testbed, especially in the combination with the indoor/outdoor capabilities. A first step is the LTE-WLAN aggregation (LWA) and LTE WLAN radio level integration with IPsec tunnel (LWIP) features, which are implemented for further experiments in the NI NS3-framework on top of the NI 802.11 and LTE PHY layer implementations [15]. Another possibility is to study joint decoding, where the same messages are spread over different PHY layers, but

combined at the receiver before the medium access control (MAC) protocol for reliable wireless networks. In addition, the in-house developed 26 GHz mmWave USRP-frontends and a 60 GHz NI based mmWave demonstrator allow the combination of sub 6 GHz with mmWave frequencies.

Further series of experimentation are possible with the HPE edge cloud computing platforms attached to the testbed. Every node is connected with individual fibers, which allows to stream the received samples to the cloud. Here Coordinated Multipoint (CoMP) and similar techniques can be evaluated in real-time, in contrast to the previous Dresden EASY-C testbed [16], where the signal processing was conducted offline. Also, the signal processing can be split for Cloud-RAN (C-RAN) experiments between antenna and cloud. As SDR and cloud are tightly interconnected, experiments exploring real-time control applications can be conducted with the testbed as described in [17]. For such purpose, a mobile robot platforms as well as FRANKA EMIKA robot arms in the laboratories are available. Here, performance comparisons of centralized infrastructure approaches versus device-to-device communications can be investigated considering some of the nodes as small cells, whereas the outdoor nodes are configured as micro cells.

III. Evaluation

In this section, we evaluate the the coverage prior to equipping the testbed with devices. For that, transmission experiments using the sensing USRPs B205mini have been carried out. In this trial, one USRP on the roof-top transmits a repeated Chirp-based sequence using the selected power amplifier, bandpass and the BS antenna. Another USRP captures the received signals on several positions as indicated in Fig. 1. The received measurements are processed offline.

A. Chirp-based Sequence

In the measurement campaign, chirp-based sequence is used due to its advantageous autocorrelation property. The discrete-time reference down-chirp is defined by the Polyphase code [18] and is arranged in the following column vector

$$\mathbf{g}_{\mathrm{d}} = \left(\exp\left(-j\pi\frac{n^2}{N}\right)\right)_{n=0,1,\cdots,N-1}. \tag{1}$$

From (1), we construct 5 subsequent down-chirps sequences as $\tilde{\mathbf{g}}_{\mathrm{d}} = \left(\mathbf{g}_{\mathrm{d}}^{\mathrm{T}}, \mathbf{g}_{\mathrm{d}}^{\mathrm{T}}, \mathbf{g}_{\mathrm{d}}^{\mathrm{T}}, \mathbf{g}_{\mathrm{d}}^{\mathrm{T}}, \mathbf{g}_{\mathrm{d}}^{\mathrm{T}}\right)^{\mathrm{T}}$, where $(\cdot)^{\mathrm{T}}$ stands for the transposition operator. Then, we define a sequence of 5 up-chirps as $\tilde{\mathbf{g}}_{\mathrm{u}} = \left(\mathbf{g}_{\mathrm{d}}^{\mathrm{H}}, \mathbf{g}_{\mathrm{d}}^{\mathrm{H}}, \mathbf{g}_{\mathrm{d}}^{\mathrm{H}}, \mathbf{g}_{\mathrm{d}}^{\mathrm{H}}, \mathbf{g}_{\mathrm{d}}^{\mathrm{H}}\right)^{\mathrm{T}}$, where $(\cdot)^{\mathrm{H}}$ stands for the conjugate transposition. Notice that the conjugate of $\mathbf{g}_{\mathrm{d}}$ in (1) changes the sign inside the exponential argument, transforming the signal into an up-chirp. The transmitted sequence is

$$\mathbf{x} = \left(\tilde{\mathbf{g}}_{\mathrm{d}}^{\mathrm{T}}, \tilde{\mathbf{g}}_{\mathrm{u}}^{\mathrm{T}}, \mathbf{0}_{5N}^{\mathrm{T}}\right)^{\mathrm{T}}, \tag{2}$$

which is composed of the 5 down-chirps, 5 up-chirps and a vector of $5N$ zeros which is given by $\mathbf{0}_{5N}$. The zero sequence is included to allow us to estimate the noise power and consequently the SNR. Additionally, we highlight that the combination of up and down-chirps can be used to estimate integer carrier frequency offset (CFO)[1], as shown in [19]. At transmitter, we simply transmit the signal of (2) repeatedly.

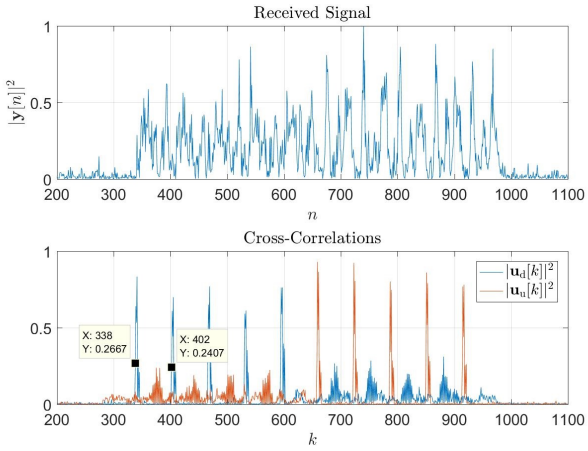

Fig. 3: Time synchronization example.

B. SNR Estimation

In order to estimate the SNR, we need to synchronize the received sequence in time-domain. First, we notice that the maximum CFO normalized to subcarrier spacing of the chirp $\mathbf{g}_{\mathrm{d}}$ is very small. In particular, it is calculated as $\phi_{\max} = \frac{f_{\mathrm{acc}} \times f_{\mathrm{c}}}{B/N} = 0.048$, where $f_{\mathrm{acc}} = 4 \times 10^{-6}$ is the frequency accuracy of the USRP B205mini's oscillator, $f_{\mathrm{c}} = 3.75$ MHz is the carrier frequency, $B = 20$ MHz is the bandwidth (or sampling rate) and $N = 64$ is the length of $\mathbf{g}_{\mathrm{d}}$. Because $\phi_{\max}$ is small, we can synchronize the sequence in time very accurately by performing the cross-correlation with the down and up-chirps, respectively, as

$$\mathbf{u}_{\mathrm{d}}[k] = \frac{1}{N}\sum_{n=0}^{N-1}\mathbf{r}[k+n]e^{-j\pi\frac{n^2}{N}},\ \mathbf{u}_{\mathrm{u}}[k] = \frac{1}{N}\sum_{n=0}^{N-1}\mathbf{r}[k+n]e^{j\pi\frac{n^2}{N}}, \tag{3}$$

We then compare $|\mathbf{u}_{\mathrm{d}}[k]|^2$ and $|\mathbf{u}_{\mathrm{u}}[k]|^2$ to a threshold γ, where $|\cdot|$ returns the absolute value of its argument. The received signal is declared synchronized if $|\mathbf{u}_{\mathrm{d}}[\hat{k}+iN]|^2 > \gamma$ and $|\mathbf{u}_{\mathrm{u}}[\hat{k}+iN+5N]|^2 > \gamma$ simultaneously for all $i = 0, 1, 2, 3, 4$. In this case, the sequence starts at $\mathbf{y}[\hat{k}]$. Figure 3 depicts the idea of using $\mathbf{u}_{\mathrm{d}}[k]$ and $\mathbf{u}_{\mathrm{p}}[k]$ for time synchronization, where we considered a fixed channel with $L = 8$ taps and SNR equal to 10 dB. One can observe that well-defined peaks appear in the cross correlation functions. More precisely, they are separated by $N = 64$ samples, as it is shown for the first two local peaks. Afterwards, we can estimate the SNR by

$$\hat{\rho} = \frac{\frac{1}{10N}\sum_{i=0}^{10N-1}|\mathbf{y}[i+\hat{k}]|^2}{\frac{1}{5N-p}\sum_{i=p}^{5N-1}|\mathbf{y}[i+\hat{k}+10N]|^2} - 1, \tag{4}$$

where the numerator in (4) contains signal plus noise, providing an estimate of both signals added. The denominator contains only noise, providing an estimate of the noise power only, where the parameter p determines a shift on where we

[1]In this work, it was not necessary to estimate the CFO due to small CFO range. This sequence is designed for more general case.

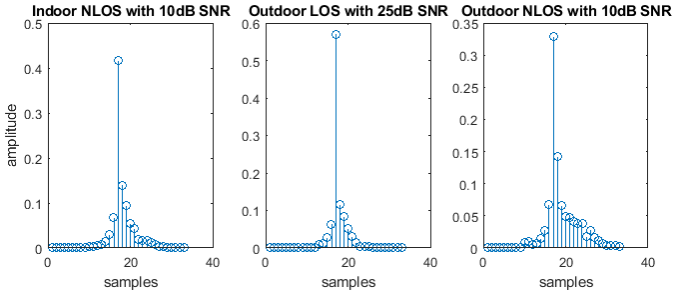

Fig. 4: Average equivalent channel impulse responses for the different categories and the averaged SNR

start estimating the noise power and is chosen to guarantee a noise only signal while estimating the noise power. Finally, we subtract 1 because the fraction provides an estimation of $(P_{\text{signal}} + P_{\text{noise}})/P_{\text{noise}}$ which equals SNR + 1, resulting in an unbiased estimation. In practice, we average the SNR estimation in (4) over several chirp sequences for refinement.

C. Channel Estimation

Before performing the channel estimation, we need to correct the CFO, otherwise the reference chirp is shifted in frequency. The CFO estimation is done by averaging the phase of the autocorrelation function as in [19],

$$\hat{\phi} = \frac{1}{6\times 2\pi}\sum_{i=1}^{3} \arg\left\{\mathbf{m}[\hat{k}+iN]\right\} + \arg\left\{\mathbf{m}[\hat{k}+iN+5N]\right\}, \tag{5}$$

where $\mathbf{m}[k] = \frac{1}{N}\sum_{n=0}^{N-1}\mathbf{y}[k+n]^{\dagger}\mathbf{y}[k+n+N]$ is the autocorrelation function and $\arg\{\cdot\}$ returns the phase of the argument. Notice that (5) averages the phase of the autocorrelation function starting from the second down and up-chirps, since the channel is not circulant over the first chirps. After CFO compensation, the channel response in the frequency domain can be estimated using the zero forcing (ZF) approach

$$\mathbf{h}_{\text{F}} = \frac{1}{8}\sum_{i=1}^{4}\frac{\mathbf{R}_{\hat{k}+iN}}{\text{FFT}\{\mathbf{g}_{\text{d}}\}} + \frac{\mathbf{R}_{\hat{k}+iN+5N}}{\text{FFT}\{\mathbf{g}_{\text{u}}\}}, \tag{6}$$

where $\mathbf{R}_q = \text{FFT}\{(\mathbf{r}[q], \mathbf{r}[q+1], \cdots, \mathbf{r}[q+N-1])\}$ is the fast Fourier transform of the received signal starting in the index q with size N. Notice that by choosing $i = \{1,2,3,4\}$, we select the portion of the signal in which the channel is circulant over the chirps, allowing us to estimate the channel in the frequency domain as (6).

D. Results

The captured channels are depicted in Figure 4. The channels are averaged for the indoor & outdoor, and for the non- & line-of-sight (LOS) case including the average SNR. In the outdoor LOS case, a single strong tap appears, as well as in the indoor case, because the weak paths are blocked by obstacles like windows or walls. Whereas in the outdoor non-LOS case, a strong tap, a weaker second tap, and a few local scattering taps are present. The average SNR for the indoor nodes for the given BS is around 9 dB. Actually, the windows have an attenuation larger than 25 dB. The yard of the institute building has a good coverage of 25 dB for mobile experiments and the coverage around the building is sufficient for experiments with 10 dB SNR. On the other hand, the indoor and outdoor coverage around the building is planned to be improved by deploying other BSs in the near future.

IV. Conclusion

The testbed presented in this paper enables the investigation of most aspects of cellular networks. The infrastructure of the testbed allows real-time experiments that benefit form having low-latency, high throughput access to FPGAs on the SDR platform and powerful host machines. With variety of indoor and outdoor nodes, it is possible to target realistic scenarios beyond the typical lab environment. The installed radio platforms are standard independent, and thus, the testbed provides more freedom for research and testing. A first field trials provides a coverage map with the expected SNRs and channel impulse responses showing the potential of the testbed in different environments. Finally, the Fed4Fire-compliance makes our testbed available for any registered user.

References

[1] G. Wunder *et al.*, "5GNOW: non-orthogonal, asynchronous waveforms for future mobile applications," *IEEE Communications Magazine*, vol. 52, no. 2, pp. 97–105, Feb 2014.

[2] G. P. Fettweis, "The tactile internet: Applications and challenges," *IEEE Vehicular Technology Magazine*, vol. 9, no. 1, pp. 64–70, March 2014.

[3] IMEC iLab.t, "w-ilab.t testbed." [Online]. Available: https://doc.ilabt.imec.be/ilabt-documentation/wilabfacility.html

[4] Connectcentre.ie, "Iris - the reconfigurable radio testbed." [Online]. Available: https://iris-testbed.connectcentre.ie/

[5] IMEC iLab.t, "Virtual wall testbed." [Online]. Available: https://doc.ilabt.imec.be/ilabt-documentation/

[6] ORBIT Consortium, "Open-access research testbed for next-generation wireless networks." [Online]. Available: http://www.orbit-lab.org/

[7] OWL Homepage, [Online]. Available: http://owl.ifn.et.tu-dresden.de/

[8] OpenStreetMap contributors, "XML dump retrieved from https://www.openstreetmap.org/map=18/51.02688/13.72289," https://www.openstreetmap.org , 2017.

[9] National Instruments, "USRP hardware driver software." [Online]. Available: https://github.com/EttusResearch/uhd

[10] X. Wang *et al.*, "28 GHz multi-beam antenna array based on a compact wideband 8x8 butler matrix," in *2018 IEEE ISAP and USNC-URSI Radio Science Meeting*, July 2018.

[11] National Instruments, "LTE application framework." [Online]. Available: http://sine.ni.com/nips/cds/view/p/lang/de/nid/213083

[12] ——, "802.11 application framework." [Online]. Available: http://sine.ni.com/nips/cds/view/p/lang/de/nid/213084

[13] M. Danneberg *et al.*, "Universal waveforms processor," in *EuCNC 2018,*, pp. 357–362.

[14] University of Piraeus Research Center, "Waveform design and benchmarking tool." [Online]. Available: http://tsl.ds.unipi.gr/wildcat/

[15] ORCA Consortium, "LWA and LWIP." [Online]. Available: http://owl.ifn.et.tu-dresden.de/NI/MultiRat-LWx.html

[16] TU Dresden, "Enablers of ambient services and systems." [Online]. Available: http://www.easy-c.de/

[17] M. Danneberg *et al.*, "Network slicing for industry 4.0 applications - initial RAN testbed results," January 2018, IEEE Softwarization.

[18] D. Chu, "Polyphase codes with good periodic correlation properties," *IEEE Trans. Inf. Theory*, vol. 18, no. 4, pp. 531–532, July 1972.

[19] S. Boumard and A. Mammela, "Robust and Accurate Frequency and TimingSynchronization Using Chirp Signals," *IEEE Trans. on Broad.*, vol. 55, no. 1, pp. 115–123, March 2009.